Robust Superhydrophobic Conical Pillars from Syringe Needle Shape to Straight Conical Pillar Shape for Droplet Pancake Bouncing

Jinlong Song[1], Liu Huang[1], Changlin Zhao[1], Song Wu[1], Hong Liu[2], Yao Lu[3], Xu Deng[4], Claire J. Carmalt[5], Ivan P. Parkin[5], Yuwen Sun[1]**

[1] Key Laboratory for Precision and Non-traditional Machining Technology of the Ministry of Education, Dalian University of Technology, Dalian 116024, P. R. China.

[2] Key Laboratory of Theoretical Chemistry of Environment Ministry of Education, South China Normal University, Guangzhou 510006, P. R. China.

[3] Department of Chemistry, School of Biological and Chemical Sciences, Queen Mary University of London, London E1 4NS, UK.

[4] Institute of Fundamental and Frontier Sciences, University of Electronic Science and Technology of China, Chengdu 610054, P. R. China.

[5] Department of Chemistry, University College London, 20 Gordon Street, London, WC1H 0AJ, UK.

ABSTRACT: Superhydrophobic conical pillars have great industrial application potential in, for example, anti-icing of aircraft wings and protecting high voltage transmission lines from freezing rain because of their droplet pancake bouncing phenomenon which is recognized to furthest reduce the liquid-solid contact time. However, there are still no methods that can large-scale fabricate robust superhydrophobic conical pillars. Here, a mold replication technology was proposed to realize the large-scale fabrication of superhydrophobic conical pillars with a high mechanical strength. An Al mold with intensive conical holes decorated with micro/nanometer-scale structures was fabricated by nanosecond laser drilling and HCl etching. The conical shape originated from a near Gaussian spatial distribution of the energy and temperature in the radial direction in the laser drilling processes. Robust superhydrophobic conical pillars from syringe needle shape to straight conical pillar shape were easily fabricated through replication from the Al mold without any extra spray of superhydrophobic nanoparticles. It was also found that although all superhydrophobic conical pillars with different shape could generate the droplet pancake bouncing, the shape had a great influence on the critical bottom space and the critical Weber number (*We*) to generate pancake bouncing. The pancake bouncing with the shortest contact time of a 68.5% reduction appeared on superhydrophobic straight conical pillars with the shape angle of 180°. Overcoming the difficulties in the large-scale fabrication and robustness of superhydrophobic conical pillars will promote practical applications of the droplet pancake bouncing phenomenon.

KEYWORDS: conical pillars, superhydrophobic, pancake bouncing, large-scale, robust

1. INTRODUCTION

Superhydrophobic surfaces which are inspired from the lotus leaf have been widely studied for more than 20 years. However, due to the continuous development of new application prospects, such as self-cleaning[1, 2], oil/water separation[3], drag-reduction[4-6], corrosion-resistance[7], anti-bacterium[8], anti-icing[9-11], fog-harvest[12-14], pumpless transport of liquid[15, 16], condensation-enhancement[17-20], and biomedical applications[21-27], superhydrophobic surfaces still attract more and more attention from the academic community. The number of papers about superhydrophobic surface increases every year with > 1670 papers indexed in the ISI Web of Science in 2018 (Figure S1). Hence, developments on superhydrophobic surfaces will be of great interest to the academic community particularly where possibilities of widespread application can be realized.

Superhydrophobic surface could effectively reduce the liquid-solid contact time compared with common hydrophilic or hydrophobic surface because of its >150° contact angle and <10° sliding angle. However, the liquid-solid contact time of a water droplet with a certain volume on a superhydrophobic flat surface is constant[28]. How to further reduce the contact time has fascinated many scientists and the investigations showed that superhydrophobic point-like macrotexture[29], micrometer-scale ridge[30-32], millimeter-scale ridge[32, 33] and submillimeter-scale conical pillars could effectively further reduce the liquid-solid contact time[34]. Among them, superhydrophobic submillimeter-scale conical pillars can produce a droplet pancake bouncing phenomenon which is recognized to furthest reduce the liquid-solid contact time. That is, the droplet pancake bouncing surface corresponds to the lowest liquid-solid contact time which can be worthy of further exploration. Additionally, only superhydrophobic submillimeter-scale conical pillars can ensure that all water droplets impacted on the solid surface detach quickly with a pancake shape from the substrate, showing great practical application potential at anti-icing from the freezing rains. How to fabricate superhydrophobic submillimeter-scale conical pillars is the key to the application of the droplet pancake bouncing phenomenon. Liu et al. developed a combined process composed of electric spark cutting, chemical oxidation, and fluoroalkylsilane modification to fabricate superhydrophobic submillimeter-scale conical pillars on a Cu substrate[34]. They first constructed conical pillars with diameter of 20-200 μm and height of 800-1200 μm and then constructed micro/nanometer-scale flower-like and needle-like structures and finally reduced the surface energy. Graeber et al. fabricated a polymer mold with conical holes by 3D printing, and then replicated submillimeter-scale conical polymeric pillars[35]. Since the surface of the pillars was too smooth, superhydrophobic PTFE nanoparticles were sprayed on top to render the submillimeter-scale conical polymeric pillars superhydrophobic. However, the aforementioned methods have certain deficiencies. The processing efficiency of electric spark cutting is very low, resulting in a time consuming and costly fabrication processes for a large-scale surface. Theoretically, mold replication technology is high efficiency, low cost, and easy in operation. However, the non-metal mold obtained by 3D printing is easy to wear out and the smooth replica needs extra spray treatment to acquire superhydrophobicity. In addition, the adhesive force between the sprayed superhydrophobic nanoparticles and the replica is low, resulting in a low mechanical strength. The reported method did not take advantage of mold replication technology and is still low efficiency and high cost. It is still an unanswered question as to how to fabricate a metal mold with intensive conical holes and how to cancel extra spray treatment but still acquire superhydrophobicity. These are important questions to decide if the mold replication technology can fabricate large-scale superhydrophobic conical pillars with high efficiency and low cost. Moreover, further exploration of whether superhydrophobic conical pillars with a larger diameter besides submillimeter-scale can generate the pancake bouncing is required.

Nanosecond laser is often used to drill holes on metal substrates because of its high efficiency and low cost. However nanosecond laser with a near Gaussian spatial distribution of the energy and temperature in the radial direction in the laser drilling processes has a fatal disadvantage for drilling holes with a high depth-diameter ratio in that conical holes often occur, which is tried to be avoided in the industry. Here, we made full use of the aforementioned disadvantages and drilled intensive conical holes on Al substrate by nanosecond laser. After HCl etching to decorate micro/nanometer-scale structures on the inner wall of the conical holes, the Al mold was obtained. Robust superhydrophobic conical pillars from syringe needle shape to straight conical pillar shape were easily fabricated through replication from the Al mold without any extra spray of superhydrophobic nanoparticles. Bouncing dynamics of an impacting water droplet shows that the replicated superhydrophobic conical pillars with different shapes and bottom diameter from submillimeter to millimeter could generate the pancake bouncing phenomenon. This developed method makes full use of the advantages of mold replication technology to fabricate large-scale superhydrophobic conical pillars with high efficiency and low cost.

2. EXPERIMENTAL

2.1 Fabrication of Superhydrophobic Conical Pillars

The fabrication processes of superhydrophobic conical pillars is shown in Figure 1. Prior to laser drilling, an aluminum (Al, purity > 99%, Alighting Co., Shanghai) plate with thickness of 2 mm was ultrasonically washed in deionized water and air-dried. Then, intensive conical holes with different shape and size (diameter, height, and space) were drilled on the Al plate in ambient condition with humidity of 30-50% and temperature of 20-25 °C by nanosecond laser (wavelength 1064 nm, pulse duration 100 ns, repetition rate 20 kHz, spot size 100 μm). The scanning speed was 500 mm/s and the scanning times for each hole was 60 times. After laser drilling, the Al plate was ultrasonically washed in deionized water and immersed in the 0.4 mol/L aqueous HCl (Alighting Co., Shanghai) solution for 2 min to construct micro/nanometer-scale structures on the inner wall of the conical holes. After another ultrasonic wash in deionized water, the Al mold was obtained. Then, polydimethylsiloxane (PDMS, Sylgard 184, Dow Corning, Germany), which was used as the representative casting body, was poured onto the Al mold and baked at 60°C for 3 h in a vacuum drying oven. The mass ratio of PDMS and cross-linker was 10:1. After knockout, the intensive conical pillars were replicated. Finally, the replica was immersed in a 1.0 wt % ethanol solution of FAS (fluoroalkylsilane, $C_8F_{13}H_4Si(OCH_2CH_3)_3$, Degussa Co., Germany) for 30 min and heated at 50 °C for 10 min. Thus, superhydrophobic conical pillars were fabricated. It is worth noting that the Al mold can be reused.

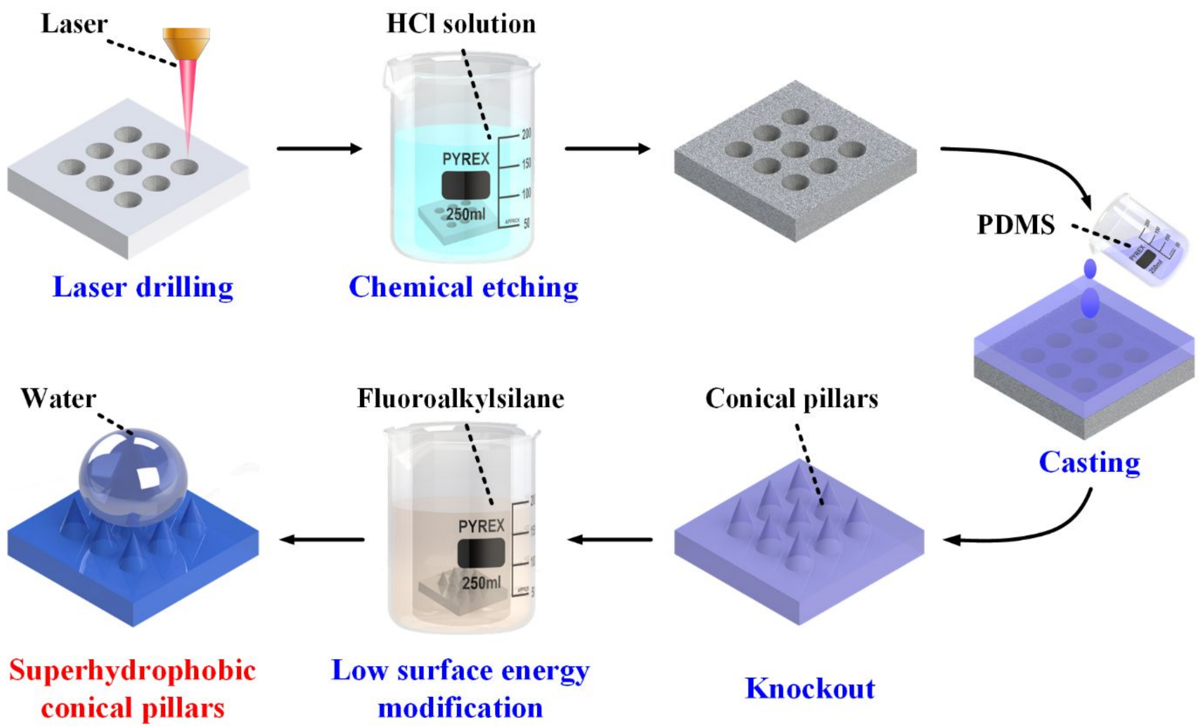

Figure 1. Schematics of the fabrication processes of superhydrophobic conical pillars.

2.2 Characterization

The micro structures and surface morphology of the samples were characterized using a scanning electron microscope (SEM, SUPRA 55 SAPPHIRE, Germany). The contact angle (CA) of a 5 μL water droplet on the samples was measured using an optical contact angle meter (Krüss, DSA100, Germany). The dynamic bouncing processes of water droplets with volume of 21 μL on the samples were characterized using a high speed camera (NAC, MEMRECAM HX-7S, Japan) at 10000 frame/s. For a water droplet, when the ratio (Q) of the lateral extension diameter (d_{jump}) at the detachment moment from the sample surface and the maximum lateral extension diameter (d_{max}) in the jumping processes is larger than 0.8, that is $Q = (d_{jump}/d_{max}) > 0.8$, the pancake bouncing is obtained[32], as shown in Figure S2. The Weber number We is defined as $We = \rho v^2 r_0/\gamma$, where ρ, v, r_0, and γ relate to the density, impact velocity, radius, and surface tension of water droplets, respectively. The bottom diameter, height, and bottom space of the conical pillars were defined as D, H, and S, as shown in Figure S3.

3. RESULTS AND DISCUSSION

It is well known that surface micro/nanometer-scale structures and low surface energy are necessary for superhydrophobicity. Although the nanosecond laser could easily drill conical holes on an Al substrate, the substrate surface was rather smooth and the inner wall of the holes was not rough enough (Figure 2(a)), resulting in that the replica substrate surface and the external surface of the replicated conical pillars were also smooth (Figure 2(b)). Such a smooth surface cannot obtain superhydrophobicity even after FAS modification. For water droplet on the replica substrate surface, the contact angle was only 138° (Figure 2(c)). For water droplet on the replicated conical pillars, the water droplet penetrated into the voids between the conical pillars, showing a typical Wenzel hydrophobic state (Figure 2(d))[36]. In order to construct micro/nanometer-scale structures on the substrate surface and the inner wall of the conical holes, after laser drilling an HCl etching process was introduced, which effectively formed the micro structures required for superhydrophobicity[37]. Figure 2(e) shows the SEM image of the Al substrate after laser drilling and HCl etching. It can be seen that the substrate surface and the inner wall of the conical holes were rough and composed of micro/nanometer-scale pits and protuberances. After replication, the replica substrate surface and the external surface of the replicated conical pillars were also rough (Figure 2(f)). With further FAS modification, superhydrophobicity was obtained. Water droplet on the replica substrate surface showed a spherical shape with contact angle of 163° (Figure 2(g)). Water droplet on the replicated conical pillars also showed a spherical shape whose bottom has a composite contact region composed of liquid-solid contact region and liquid-air contact region (Figure 2(h)), showing Cassie-Baxter superhydrophobic state. Thus, superhydrophobic conical pillars were fabricated.

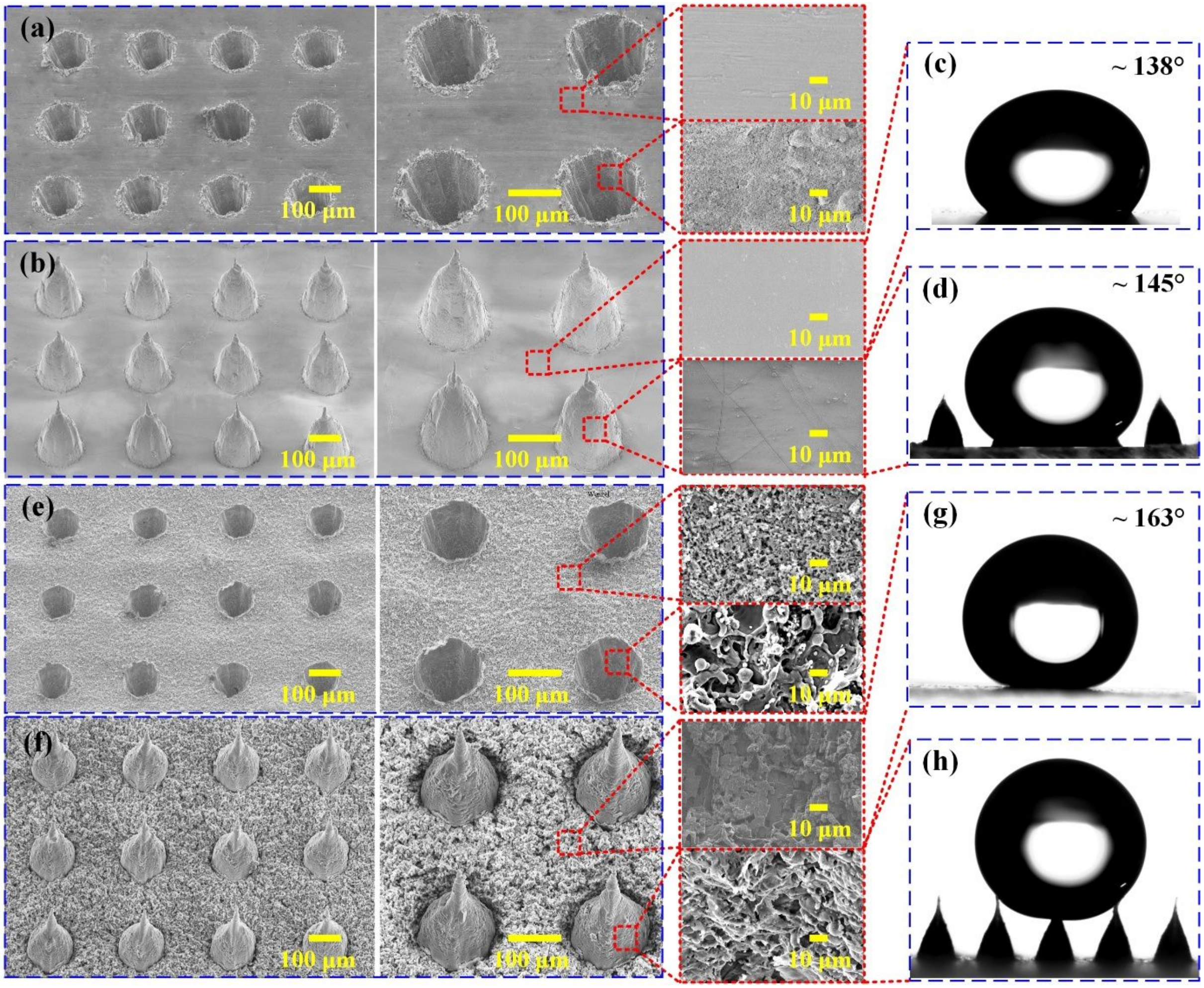

Figure 2. Surface morphology of the Al mold and the replica. (a) SEM images with different magnifications of the Al mold obtained by laser drilling. (b) SEM images with different magnifications of the conical pillars with *D*=210 μm, *H*=640 μm, and *S*=180 μm replicated from the Al mold obtained by laser drilling. (c) The replica substrate surface was smooth and had a water CA of 138°. (d) The surface of the replicated conical pillars was not rough enough and water droplet on it showed a Wenzel hydrophobic state. (e) SEM images with different magnifications of the Al mold obtained by laser drilling and HCl etching. (f) SEM images with different magnifications of the conical pillars with *D*=210 μm, *H*=640 μm, and *S*=180 μm replicated from the Al mold obtained by laser drilling and HCl etching. (g) The replica substrate surface was rough and had a water CA of 163°. (h) The surface of the replicated conical pillars was rough and water droplet on it showed a Cassie-Baxter superhydrophobic state. The processing

power of nanosecond laser for the conical holes in (a) and (e) was 9 W.

In the replication processes of the conical pillars by the Al mold, it was surprising to find that the conical pillars with special shape were obtained besides the common straight conical pillars simply by adjusting the processing power of the nanosecond laser. In order to describe the conical pillars more clearly, the conical pillar was divided into two parts composed of head part and base part, as shown in Figure 3 (a). A shape angle β was then defined, which is the angle between the tangent lines along conical pillars contour at the cross point of head part and base part. The influence of the processing power P of the nanosecond laser on the β at different bottom diameter is shown in Figure 3(b). It can be seen that the β at different bottom diameter changes with the same trend that the β increased with the increase of the processing power P. The conical pillar changed from syringe needle shape with the β of 139-147° to straight conical pillar shape with the β of 180° with the increase of the β, as shown in Figure 3(c) and 3(d). It was also observed that the required processing power for the straight conical pillar increased with the increase of the bottom diameter. All the conical pillars with different shape replicated from the Al mold obtained by laser drilling and HCl etching show superhydrophobicity with CA > 160°.

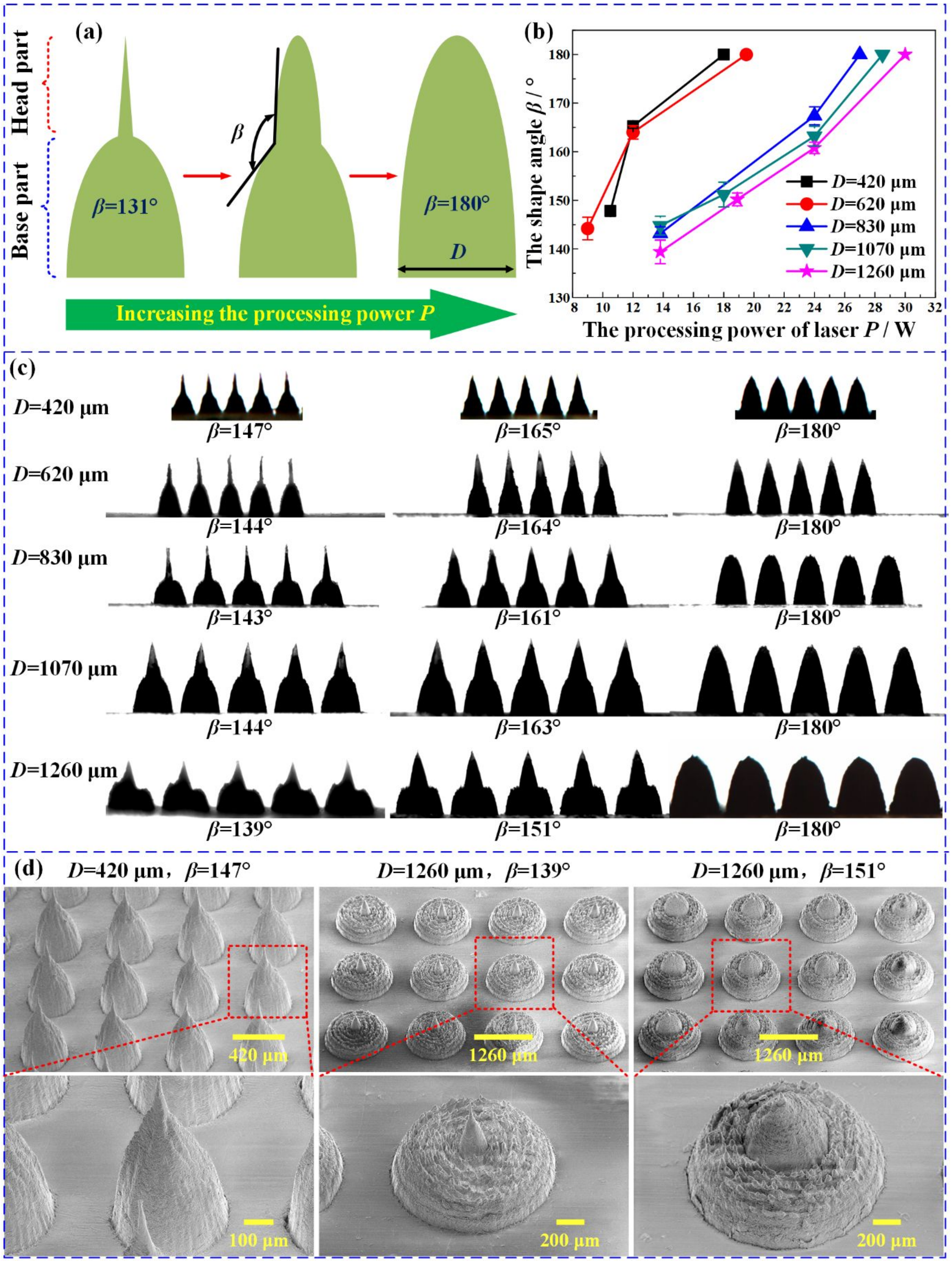
(a)
Head part
Base part
β=131°
β
β=180°
D
Increasing the processing power P
(b)
The shape angle β / °
The processing power of laser P / W
D=420 μm
D=620 μm
D=830 μm
D=1070 μm
D=1260 μm
(c)
D=420 μm
β=147°
β=165°
β=180°
D=620 μm
β=144°
β=164°
β=180°
D=830 μm
β=143°
β=161°
β=180°
D=1070 μm
β=144°
β=163°
β=180°
D=1260 μm
β=139°
β=151°
β=180°
(d) D=420 μm，β=147°
D=1260 μm，β=139°
D=1260 μm，β=151°
420 μm
1260 μm
1260 μm
100 μm
200 μm
200 μm

Figure 3. The influence of the processing power of the nanosecond laser on the shape of the replicated conical pillars. (a) The schematics of the evolution processes of the shape of the replicated conical pillars. (b) The influence of the processing power P of the nanosecond laser on the β at different bottom diameters. (c) The side view of the replicated conical pillars with different β at different bottom diameter. (d) SEM images with different magnifications of the replicated conical pillars with 3 typical shapes.

The conical pillar with different shape angle β was replicated from the conical hole with different shape angle β. Figure 4 provides an explanation for the conical hole with different shape angle β. Since the laser spot is often much smaller than the required hole diameter, the laser spot often performs spiral scanning from the inside to the outside and then from the outside to inside again for each scanning time, as shown in Figure 4(a). The total scanning times can be set by manipulator and was set at 60 times here. In the drilling processes, energy and temperature were a near Gaussian spatial distribution in the radial direction that is the energy and temperature presented a decreasing trend from the center to the edge of the hole[38, 39]. The higher energy and temperature indicate a faster removing velocity of the Al material. Thus, a conical hole was formed. For the low processing power, the area of high energy and temperature near the hole center is small, resulting in the syringe needle shape with the small β. With the increase of the processing power, the area of high energy and temperature near the hole center became larger gradually, resulting in a larger β. Thus the straight conical pillar with the β of 180° was eventually formed, as shown in Figure 4(b). Therefore, for the hole with certain diameter, the shape angle β was determined by the processing power. In addition, similar to β, the depth of the hole with certain diameter was also determined by the processing power, as shown in Figure S4.

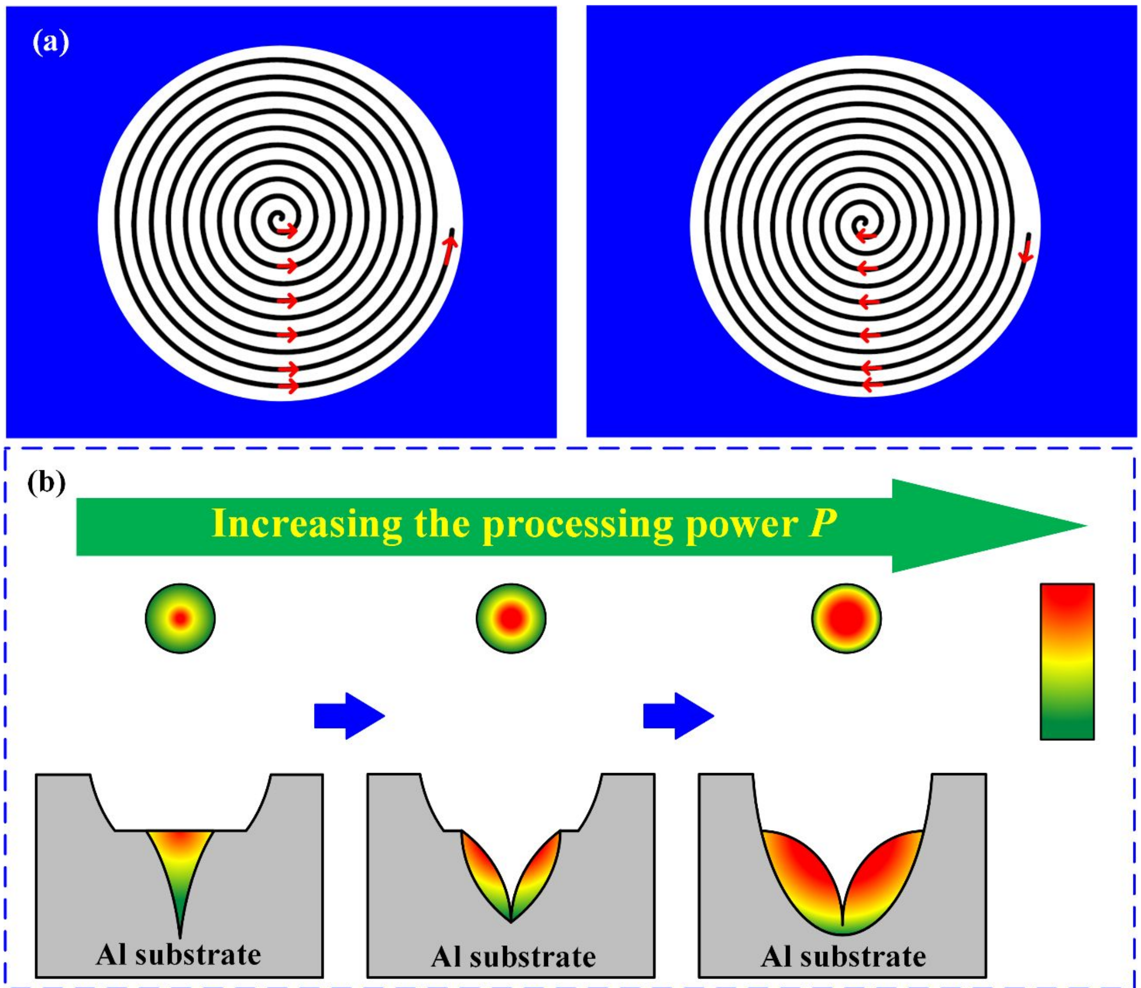

Figure 4. The schematics of the trajectory of the laser spot for each scanning time (a) and the schematics of the variation of the area of high energy and temperature near the hole center with the processing power of the laser (b). The gradual change of the color from green to red indicates the increase of the temperature.

The dynamic behavior of an impacting water droplet on superhydrophobic conical pillars with different shape was then studied in order to explore if the pancake bouncing phenomenon could occur on superhydrophobic conical pillars replicated from Al mold. For a superhydrophobic flat surface, an impacting water droplet with volume of 21 μL and *We* of 14 spread laterally first to a thin film, then recoiled, and finally detached from the substrate with an elongated shape, as shown in Figure S5 and Video S1. The total liquid-solid contact time was 22.7 ms. However, in contrast to superhydrophobic flat surface, the dynamic behavior of an impacting water droplet on superhydrophobic conical pillars was completely changed. Figure S6 and 5 shows the bouncing processes of water droplet with volume of 21 μL on superhydrophobic conical pillars with different bottom diameter D (S=210 μm and β=180°) at We=14. The impacting water droplet also spread laterally first to a thin film, then recoiled, but finally detached from the substrate with a pancake shape and a reduced liquid-solid contact time. It is also worth noting that all superhydrophobic conical pillars with the bottom diameters from 180-1260 μm could generate the pancake bouncing phenomenon with $t_{contact}$ smaller than 10.7 ms and Q larger than 0.81. The pancake bouncing with the shortest contact time and a 68.5% reduction ($t_{contact}$=7.1 ms, Q=0.91) in contact time compared with the conventional bouncing occurred at D=420 μm (Video S2).

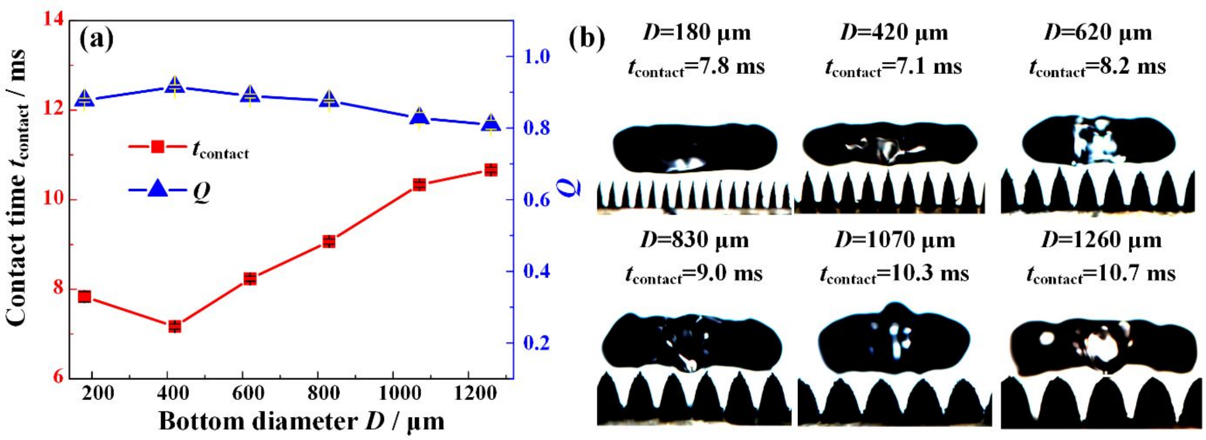

Figure 5. Variations of the liquid-solid contact time $t_{contact}$ and Q of a water droplet (21 μL) with the bottom diameter D of superhydrophobic conical pillars (S=210 μm and β=180°) at We=14 (a) and the detachment moment of the water droplet impacting on superhydrophobic conical pillars with different D (b).

The influence of the bottom space S and shape angle β of superhydrophobic conical pillars on the liquid-solid contact time $t_{contact}$ and Q was then studied. The bottom diameter D, volume of water droplet and We, were 420 μm, 21 μL and 14, respectively. As shown in Figures 6(a) and 6(b), when the bottom space *S* was small, all superhydrophobic conical pillars with different shape angle β generated the pancake bouncing phenomenon with a small $t_{contact}$ and a large Q. With the increase of *S*, the bouncing dynamics on all superhydrophobic conical pillars with different shape angle β were transformed into the conventional bouncing. However, the critical bottom space *S* to generate the pancake bouncing was different for superhydrophobic conical pillars with different β. The larger β results in a larger critical *S* for the pancake bouncing. The critical *S* to generate the pancake bouncing for superhydrophobic conical pillars (*D*=420 μm) with β of 147°, 165°, and 168° were 90 μm, 210 μm, and 290 μm, respectively. We also found that although all superhydrophobic conical pillars with different β can generate the pancake bouncing, the liquid-solid contact time $t_{contact}$ decreased with the increase of β, while Q increased with the increase of β. As shown in Figure 6(c), for *S*=90 μm, the ($t_{contact}$, Q) for the β of 147°, 165°, and 168° were (9.5 ms, 0.81), (8.3 ms, 0.87), and (7.1 ms, 0.92), respectively.

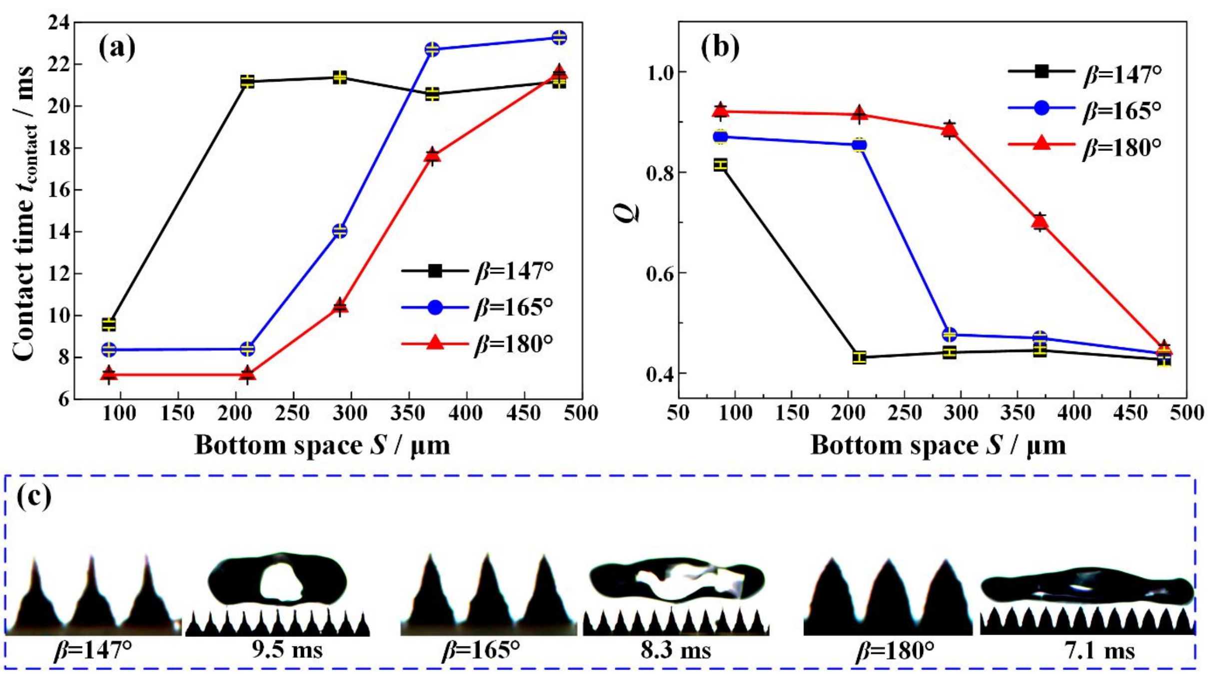

Figure 6. Variations of the liquid-solid contact time $t_{contact}$ (a) and Q (b) of a water droplet (21 μL) with the bottom space S of superhydrophobic conical pillars with different β (D=420 μm) at We=14. (c) The detachment moment of the water droplet impacting on superhydrophobic conical pillars with different β.

The influence of We on the liquid-solid contact time $t_{contact}$ and Q for superhydrophobic conical pillars with different β was also studied. Figures 7(a) and 7(b) show the variation of $t_{contact}$ and Q with We on superhydrophobic conical pillars with different β. The bottom diameter D was 420 μm, the bottom space S was 90 μm, and the volume of the water droplet was 21 μL. We found a step-like variation of $t_{contact}$ and Q with We. When the We was smaller than a critical value, a large $t_{contact}$ and a small Q remained stable, indicating the conventional bouncing. When the We increased into the critical value, the $t_{contact}$ decreased sharply and the Q increased sharply. The conventional bouncing was completely transferred into the pancake bouncing. With the further increase of We, $t_{contact}$ and Q remained stable. The critical We to generate the pancake bouncing decreased with the increase of the β and was 14, 11.6, and 9.3 for the β of 147°, 165°, and 180°, respectively. Further, in agreement with Figure 5, although all superhydrophobic conical pillars with different β can generate the pancake bouncing with We > the critical value, the $t_{contact}$ decreased with the increase of the β, while Q increased with the increase of the β.

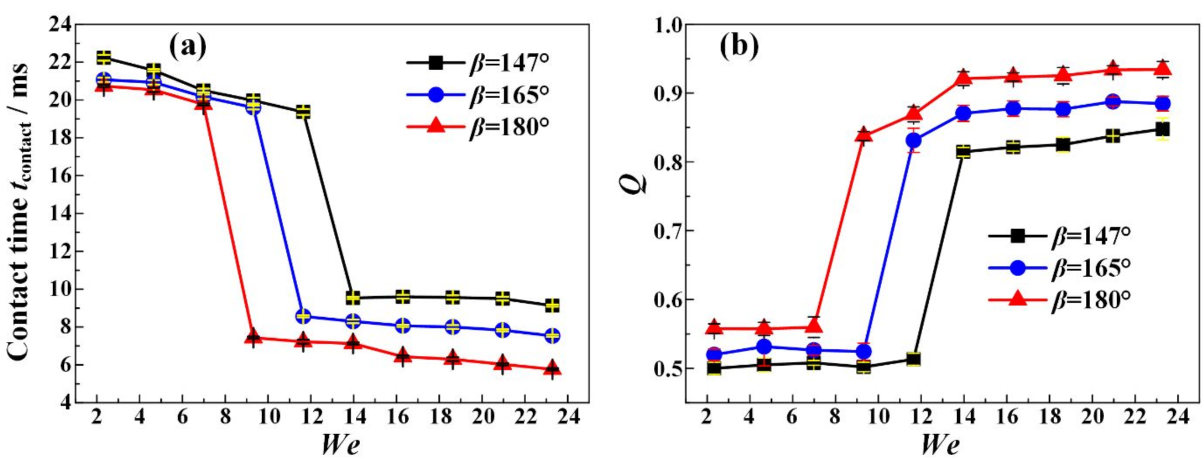

Figure 7. Variations of the liquid-solid contact time $t_{contact}$ (a) and Q (b) of a water droplet (21 μL) with the We on superhydrophobic conical pillars with different β (D=420 μm and S=90 μm).

Apart from the observed pancake bouncing of droplet with room temperature (~ 20°C), we have also tested the dynamic bouncing processes of cold and hot water droplets on superhydrophobic conical pillars. After all, anti-icing was one of the important application prospects of the droplet pancake bouncing surface. Figure S7 shows the bouncing processes of water droplets with temperature of 2°C, 5°C, 20°C, 50°C and 70°C on superhydrophobic conical pillars with D=420 μm, S=90 μm, and β=180° at We=19. All water droplets with low temperature as well as high temperature also showed a typical pancake bouncing with $t_{contact}$ ~ 4.9 ms, indicating possible application in the freezing and high temperature environment.

Since the pancake bouncing of a water droplet can occur on the replicated superhydrophobic conical pillars from the laser-drilled Al mold, we explored if the method developed here could be realized for the large-scale fabrication. We first drilled the intensive conical holes by laser on the Al substrate with an area of 80 mm×80 mm. After chemical etching, the large-scale Al mold was obtained (Figure 8(a)). Then, the PDMS conical pillars (D=830 μm, S=90 μm, and β=180°) with area of 80 mm × 80 mm were replicated. After FAS modification, superhydrophobic conical pillars with area of 80 mm × 80 mm were obtained, as shown in Figure 8(b).

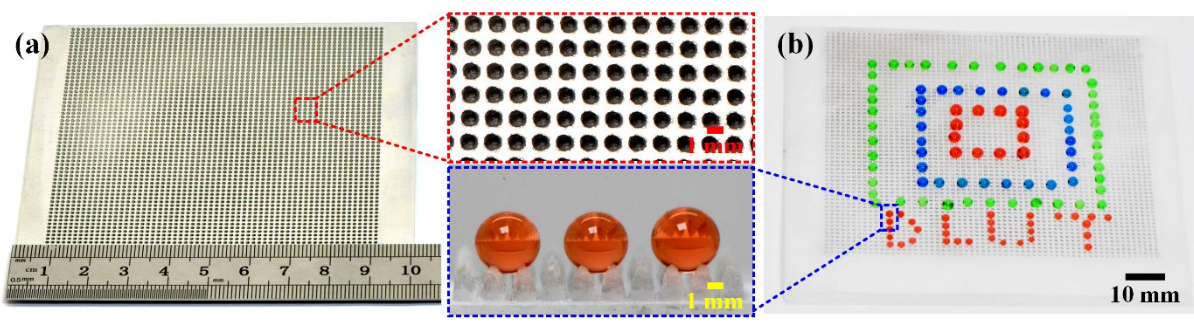

Figure 8. Digital photo of the large-scale Al mold with intensive conical holes (a) and the replicated superhydrophobic conical pillars with D=830 μm, S=90 μm, and β=180° (b). The area of the mold and sample was 80 mm × 80 mm.

To show the higher mechanical strength and robustness of superhydrophobic conical pillars obtained by our method compared with that obtained by spraying superhydrophobic nanoparticles, we scratched two types of samples by steel ruler with thickness of 200 μm, as shown in Figure S8. Figures 9(a_1) and 9(b_1) show the SEM images of superhydrophobic conical pillars replicated from the laser-drilled and HCl-etched Al mold before and after steel ruler scratch for 20 times. No changes was observed on the surface morphology and the impacting water droplets showed the pancake bouncing phenomenon both on superhydrophobic conical pillars before and after scratch, as shown in Figures 9(a_2) and 9(b_2). Figures 9(c_1) and 9(d_1) show the SEM images of superhydrophobic conical pillars obtained by replication from the laser-drilled Al mold and spraying commercial *Never-wet* superhydrophobic nanoparticles before and after steel ruler scratch for 3 times. Before scratch, the replica substrate surface and the external surface of the replicated conical pillars were coated with nanoparticles and the impacting water droplet showed the pancake bouncing phenomenon (Figure 9(c_2)). After scratch, the nanoparticles were scraped and left some smooth regions on the substrate surface. Superhydrophobicity and the pancake bouncing phenomenon were also lost and the impacting water droplets even could not detach from the scratched conical pillars, as shown in Figure 9(d_2) and Video S3. The poor adhesive force between the sprayed superhydrophobic nanoparticles and the replica resulted in poor mechanical strength. Therefore, the cancel of extra spray treatment in our method greatly improve the mechanical strength and robustness of superhydrophobic conical pillars.

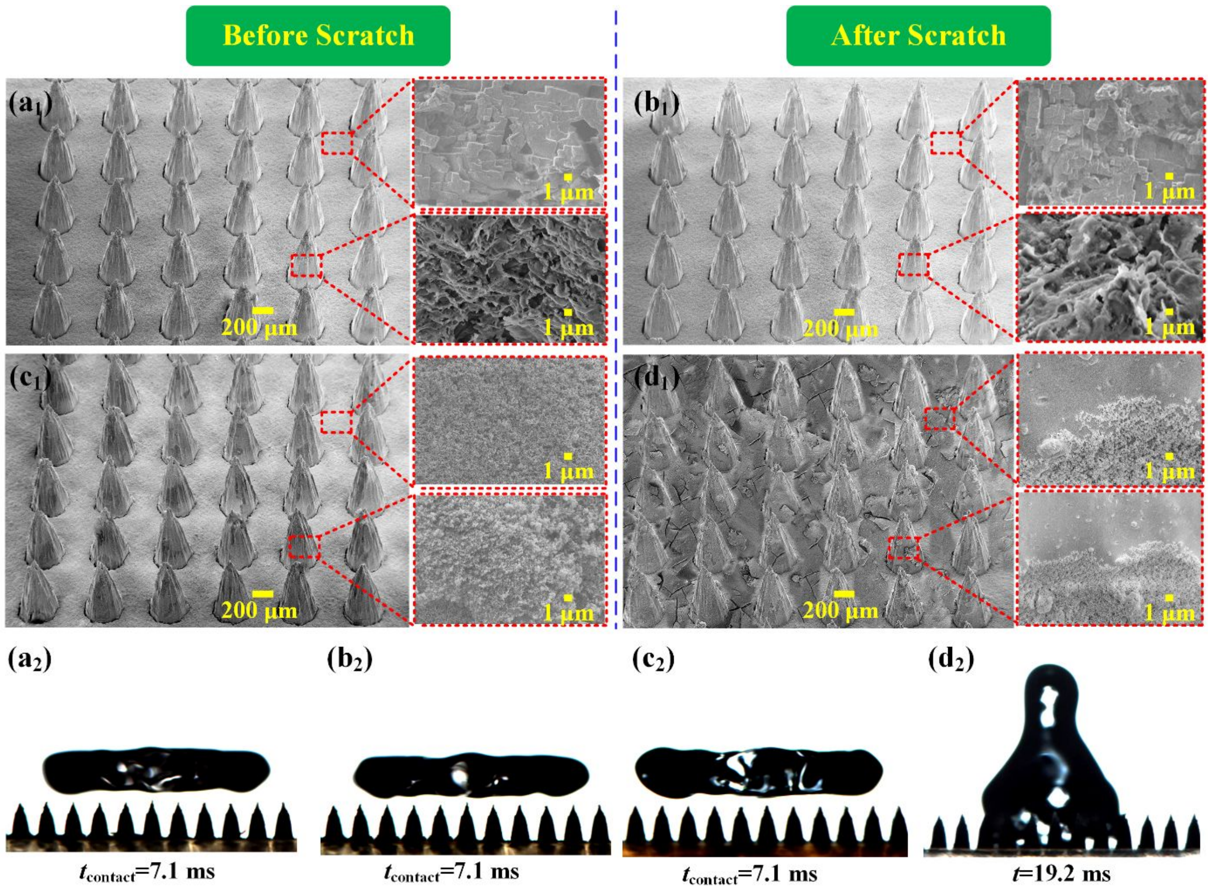

Figure 9. Surface morphology of superhydrophobic conical pillars and bouncing state of an impacting water droplet on them before and after scratch. (a_1) SEM images with different magnifications of superhydrophobic conical pillars replicated from the laser-drilled and HCl-etched Al mold and (a_2) the detachment moment of a water droplet (21 μL) impacting on them at *We*=14. (b_1) SEM images with different magnifications of superhydrophobic conical pillars replicated from the laser-drilled and HCl-etched Al mold after scratch for 20 times and (b_2) the detachment moment of a water droplet (21 μL) impacting on them at *We*=14. (c_1) SEM images with different magnifications of superhydrophobic conical pillars obtained by replication from the laser-drilled Al mold and spraying commercial *Never-wet* superhydrophobic nanoparticles and (c_2) the detachment moment of a water droplet (21 μL) impacting on them at *We*=14. (d_1) SEM images with different magnifications of superhydrophobic conical pillars obtained by replication from the laser-drilled Al mold and spraying commercial *Never-wet*

superhydrophobic nanoparticles after scratch for 3 times and (d_2) an impacting water droplet (21 μL, *We*=14) on them could not detach from the surface. The *D*, *H*, *S*, and β of superhydrophobic conical pillars were 420 μm, 830 μm, 210 μm, and 180°, respectively.

4. CONCLUSION

In summary, an Al mold with intensive conical holes decorated with micro/nanometer-scale structures were fabricated by nanosecond laser drilling and HCl etching. Through the replication of the Al mold, robust superhydrophobic conical pillars with different shapes ranging from syringe needle shape to straight conical pillar shape were easily fabricated without requiring any spray of superhydrophobic nanoparticles. The formation mechanism of the aforementioned different shape is attributed to the near Gaussian spatial distribution of energy and temperature in the radial direction in the laser drilling processes, which results in a shape that can be controlled by the processing power of the laser. We then systemically studied the influence of bottom diameter, bottom space, shape angle, and Webber number (*We*) on the contact time and bouncing shape of the impacting water droplets. It was revealed that superhydrophobic conical pillars with different shape and bottom diameter from submilimeter to millimeter could generate the pancake bouncing phenomenon. However, the critical bottom space and the critical *We* to generate the pancake bouncing was affected largely by the shape angle. The critical bottom space increased while the critical *We* decreased with the increase of the shape angle. In addition, the liquid-solid contact time for the pancake bouncing decreased with the increase of the shape angle and the shortest contact time with a 68.5% reduction appeared on superhydrophobic straight conical pillars with the shape angle of 180°. This mold replication technology is easily extended to large-scale fabrication of robust superhydrophobic conical pillars, which will promote the practical applications of the droplet pancake bouncing phenomenon.

AUTHOR INFORMATION

Corresponding Author

*E-mail: Yuwen Sun (ywsun@dlut.edu.cn), Hong Liu (hongliu@m.scnu.edu.cn)

Notes

The authors declare no competing financial interest.

ACKNOWLEDGEMENT

This project was financially supported by National Natural Science Foundation of China (NSFC, 51605078, 21774051), Young Elite Scientists Sponsorship Program by CAST (YESS, 2017QNRC001), and Aviation Science Fund (2017ZE63012), and The National Key Research and Development Program of China (2018YFB2001402). IPP and CJC thank EPSRC for grant EP/L015862/1. Yao Lu acknowledges the financial support from the QMUL-SBCS start up.

SUPPORTING INFORMATION

The number of papers about superhydrophobic surface indexed in the ISI Web of Science; schematics of the bouncing processes of a water droplet on the superhydrophobic surface; schematics of superhydrophobic conical pillars; variations of the hole depth, shape angle β with the hole diameter and the processing power of the laser; selected snapshots of a water droplet impacting on superhydrophobic flat surface at *We*=14; selected snapshots of a water droplet impacting on superhydrophobic conical pillars with different bottom diameter *D* at *We*=14; selected snapshots of water droplets with different temperature impacting on superhydrophobic conical pillars; schematics of steel ruler scratch on superhydrophobic conical pillars (PDF)

The bouncing dynamics of a water droplet impacting on superhydrophobic flat surface at *We*=14 (AVI)

The bouncing dynamics of a water droplet impacting on superhydrophobic conical pillars with *D*=420 μm, *S*=210 μm, *H*=830 μm, and β=180° at *We*=14 (AVI)

The bouncing dynamics of a water droplet impacting on Never-wet spray coated superhydrophobic conical pillars before and after steel ruler scratch for 3 times (AVI)

REFERENCES

(1) Lu, Y.; Sathasivam, S.; Song, J.; Crick, C. R.; Carmalt, C. J.; Parkin, I. P. Robust Self-Cleaning Surfaces that Function When Exposed to Either Air or Oil. *Science* **2015**, 347, 1132-1135.

(2) Wang, T.; Si, Y.; Luo, S.; Dong, Z.; Jiang, L. Wettability Manipulation of Overflow Behavior via Vesicle Surfactant for Water-Proof Surface Cleaning. *Mater. Horiz.* **2019**, 6, 294-301.

(3) Ge, J.; Shi, L.; Wang, Y.; Zhao, H.; Yao, H.; Zhu, Y.; Zhang, Y.; Zhu, H.; Wu, H.; Yu, S. Joule-Heated Graphene-Wrapped Sponge Enables Fast Clean-Up of Viscous Crude-Oil Spill. *Nat. Nanotech.* **2017**, 12, 434-440.

(4) Hu, H.; Wen, J.; Bao, L.; Jia, L.; Song, D.; Song, B.; Pan, G.; Scaraggi, M.; Dini, D.; Xue, Q.; Zhou, F. Significant and Stable Drag Reduction with Air Rings Confined by Alternated Superhydrophobic and Hydrophilic Strips. *Sci. Adv.* **2017**, 3, e1603288.

(5) Saranadhi, D.; Chen, D.; Kleingartner, J. A.; Srinivasan, S.; Cohen, R. E.; McKinley, G. H. Sustained Drag Reduction in a Turbulent flow Using a Low-Temperature Leidenfrost Surface. *Sci. Adv.* **2016**, 2, e1600686-e1600686.

(6) Vakarelski, I. U.; Klaseboer, E.; Jetly, A.; Mansoor, M. M.; Aguirre-Pablo, A. A.; Chan, D. Y. C.; Thoroddsen, S. T. Self-Determined Shapes and Velocities of Giant Near-Zero Drag Gas Cavities. *Sci. Adv.* **2017**, 3, e1701558.

(7) Xiao, F.; Yuan, S.; Liang, B.; Li, G.; Pehkonen, S. O.; Zhang, T. Superhydrophobic CuO Nanoneedle-Covered Copper Surfaces for Anticorrosion. *J. Mater. Chem. A* **2015**, 3, 4374-4388.

(8) Jiang, J.; Zhang, H.; He, W.; Li, T.; Li, H.; Liu, P.; Liu, M.; Wang, Z.; Wang, Z.; Yao, X. Adhesion of Microdroplets on Water-Repellent Surfaces toward the Prevention of Surface Fouling and Pathogen

Spreading by Respiratory Droplets. *ACS Appl. Mater. Interfaces* **2017**, 9, 6599-6608.

(9) Lo, C.; Sahoo, V.; Lu, M. Control of Ice Formation. *ACS Nano* **2017**, 11, 2665-2674.

(10) Wang, L.; Gong, Q.; Zhan, S.; Jiang, L.; Zheng, Y. Robust Anti-Icing Performance of a Flexible Superhydrophobic Surface. *Adv. Mater.* **2016**, 28, 7729-7735.

(11) Zhan, X.; Yan, Y.; Zhang, Q.; Chen, F. A Novel Superhydrophobic Hybrid Nanocomposite Material Prepared by Surface-Initiated AGET ATRP and its Anti-Icing Properties. *J. Mater. Chem. A* **2014**, 2, 9390-9399.

(12) Hou, Y.; Shang, Y.; Yu, M.; Feng, C.; Yu, H.; Yao, S. Tunable Water Harvesting Surfaces Consisting of Biphilic Nanoscale Topography. *ACS Nano* **2018**, 12, 11022-11030.

(13) Bai, H.; Wang, L.; Ju, J.; Sun, R.; Zheng, Y.; Jiang, L. Efficient Water Collection on Integrative Bioinspired Surfaces with Star-Shaped Wettability Patterns. *Adv. Mater.* **2014**, 16, 5025-5030.

(14) Zhang, L.; Wu, J.; Hedhili, M. N.; Yang, X.; Wang, P. Inkjet Printing for Direct Micropatterning of a Superhydrophobic Surface: Toward Biomimetic Fog Harvesting Surfaces. *J. Mater. Chem. A* **2015**, 3, 2844-2852.

(15) Ghosh, A.; Ganguly, R.; Schutzius, T. M.; Megaridis, C. M. Wettability Patterning for High-Rate, Pumpless Fluid Transport on Open, Non-Planar Microfluidic platforms. *Lab Chip* **2014**, 14, 1538-1550.

(16) Huang, S.; Song, J.; Lu, Y.; Chen, F.; Zheng, H.; Yang, X.; Liu, X.; Sun, J.; Carmalt, C. J.; Parkin, I. P.; Xu, W. Underwater Spontaneous Pumpless Transportation of Nonpolar Organic Liquids on Extreme Wettability Patterns. *ACS Appl. Mater. Interfaces* **2016**, 8, 2942-2949.

(17) Gong, X.; Gao, X.; Jiang, L. Recent Progress in Bionic Condensate Microdrop Self-Propelling Surfaces. *Adv. Mater.* **2017**, 29, 1703002.

(18) Wang, R.; Zhu, J.; Meng, K.; Wang, H.; Deng, T.; Gao, X.; Jiang, L. Bio-Inspired Superhydrophobic

Closely Packed Aligned Nanoneedle Architectures for Enhancing Condensation Heat Transfer. *Adv. Funct. Mater.* **2018**, 28, 1800634.

(19) Cai, S. Q.; Bhunia, A. Superhydrophobic Condensation Enhanced by Conical Hierarchical Structures. *J. Phys. Chem. C* **2017**, 121, 10047-10052.

(20) He, M.; Ding, Y.; Chen, J.; Song, Y. Spontaneous Uphill Movement and Self Removal of Condensates on Hierarchical Tower-Like Arrays. *ACS Nano* **2016**, 10, 9456-9462.

(21) Guan, F.; Zhang, J.; Tang, H.; Chen, L.; Feng, X. An Enhanced Enzymatic Reaction Using a Triphase System Based on Superhydrophobic Mesoporous Nanowire Arrays. *Nanoscale Horiz.* **2019**, 4, 231-235.

(22) Jokinen, V.; Kankuri, E.; Hoshian, S.; Franssila, S.; Ras, R. H. A. Superhydrophobic Blood-Repellent Surfaces. *Adv. Mater.* **2018**, 30, 1705104.

(23) Tronser, T.; Popova, A. A.; Jaggy, M.; Bastmeyer, M.; Levkin, P. A. Droplet Microarray Based on Patterned Superhydrophobic Surfaces Prevents Stem Cell Differentiation and Enables High-Throughput Stem Cell Screening. *Adv. Healthc. Mater.* **2017**, 6, 1700622.

(24) Ueda, E.; Feng, W.; Levkin, P. A. Superhydrophilic-Superhydrophobic Patterned Surfaces as High-Density Cell Microarrays: Optimization of Reverse Transfection. *Adv. Healthc. Mater.* **2016**, 5, 2646-2654.

(25) Popova, A. A.; Schillo, S. M.; Demir, K.; Ueda, E.; Nesterov-Mueller, A.; Levkin, P. A. Droplet-Array (DA) Sandwich Chip: A Versatile Platform for High-Throughput Cell Screening Based on Superhydrophobic-Superhydrophilic Micropatterning. *Adv. Mater.* **2015**, 27, 5217-5222.

(26) Xu, L.; Chen, Y.; Yang, G.; Shi, W.; Dai, B.; Li, G.; Cao, Y.; Wen, Y.; Zhang, X.; Wang, S. Ultratrace DNA Detection Based on the Condensing-Enrichment Effect of Superwettable Microchips. *Adv. Mater.* **2015**, 27, 6878-6884.

(27) Seo, J.; Lee, J. S.; Lee, K.; Kim, D.; Yang, K.; Shin, S.; Mahata, C.; Jung, H. B.; Lee, W.; Cho, S.; Lee, T. Switchable Water-Adhesive, Superhydrophobic Palladium-Layered Silicon Nanowires Potentiate the Angiogenic Efficacy of Human Stem Cell Spheroids. *Adv. Mater.* **2014**, 26, 7043-7050.

(28) Richard, D.; Clanet, C.; Quéré, D. Surface phenomena - Contact Time of a Bouncing Drop. *Nature* **2002**, 417, 811.

(29) Chantelot, P.; Moqaddam, A. M.; Gauthier, A.; Chikatamarla, S. S.; Clanet, C.; Karlin, I. V.; Quéré, D. Water Ring-Bouncing on Repellent Singularities. *Soft Matter* **2018**, 14, 2227-2233.

(30) Bird, J. C.; Dhiman, R.; Kwon, H.; Varanasi, K. K. Reducing the Contact Time of a Bouncing Drop. *Nature* **2014**, 505, 385-388.

(31) Gauthier, A.; Symon, S.; Clanet, C.; Quéré, D. Water Impacting on Superhydrophobic Macrotextures. *Nat. Commun.* **2015***, 6*, 8001.

(32) Guo, C.; Sun, J.; Sun, Y.; Wang, M.; Zhao, D. Droplet Impact on Cross-Scale Cylindrical Superhydrophobic Surfaces. *Appl. Phys. Lett.* **2018**, 112, 263702.

(33) Liu, Y.; Andrew, M.; Li, J.; Yeomans, J. M.; Wang, Z. Symmetry Breaking in Drop Bouncing on Curved Surfaces. *Nat. Commun.* **2015**, 6, 10034.

(34) Liu, Y.; Moevius, L.; Xu, X.; Qian, T.; Yeomans, J. M.; Wang, Z. Pancake Bouncing on Superhydrophobic Surfaces. *Nat. Phys.* **2014**, 10, 515-519.

(35) Graeber, G.; Kieliger, O. B. M.; Schutzius, T. M.; Poulikakos, D. 3D-Printed Surface Architecture Enhancing Superhydrophobicity and Viscous Droplet Repellency. *ACS Appl. Mater. Interfaces* **2018**, 10, 43275-43281.

(36) Liu, H.; Wang, Y.; Huang, J.; Chen, Z.; Chen, G.; Lai, Y. Bioinspired Surfaces with Superamphiphobic Properties: Concepts, Synthesis, and Applications. *Adv. Funct. Mater.* **2018**, 28, 1707415.

(37) Li, X.; Zhang, Q.; Guo, Z.; Shi, T.; Yu, J.; Tang, M.; Huang, X. Fabrication of Superhydrophobic Surface with Improved Corrosion Inhibition on 6061 Aluminum Alloy Substrate. *Appl. Surf. Sci.* **2015**, 342, 76-83.

(38) Yang, Y.; Chen, Z.; Zhang, Y. Melt Flow and Heat Transfer in Laser Drilling. *Int. J. Therm. Sci.* **2016**, 107, 141-152.

(39) Shuja, S. Z.; Yilbas, B. S. Laser Produced Melt Pool: Influence of Laser Intensity Parameter on Flow Field in Melt Pool. *Optics Laser Technol.* **2011**, 43, 767-775.

For Table of Contents Only